Scripta Materialia 138 (2017) 105–108

Contents lists available at ScienceDirect

Scripta Materialia

journal homepage: www.elsevier.com/locate/scriptamat

Regular Article

Difference in thermodynamics between ferrite and martensite in the Fe-Ni system

Nobuo Nakada [a,*], Naoki Kusunoki [b], Masanori Kajihara [a], Junichi Hamada [c]

[a] Department of Materials Science and Engineering, Tokyo Institute of Technology, 4259, Nagatsuta-cho, Midori-ku, Yokohama 226-8503, Japan
[b] Department of Materials Science and Engineering, Tokyo Institute of Technology, Japan [1]
[c] Nippon Steel & Sumikin Stainless Steel Corp, 3434, Shimada, Hikari City, Yamaguchi 743-8550, Japan

ARTICLE INFO

Article history:
Received 1 May 2017
Received in revised form 31 May 2017
Accepted 31 May 2017

Keywords:
Iron nickel
Martensite
Ferrite
Elastic strain energy
Recrystallization

ABSTRACT

Very fine duplex microstructure composed of recrystallized-ferrite and reversed-austenite was developed by prior cold rolling and subsequent intercritical annealing in binary Fe-Ni alloys. The equilibrium austenite fraction in the recrystallized-ferrite matrix was much smaller than that in the tempered-martensite matrix, which demonstrates that martensite is less stable than ferrite even though they have the same crystal structure of body-centered cubic. The difference in molar Gibbs energy between ferrite and martensite attributed to elastic strain energy in the martensite but not to lattice defects caused by lattice invariant deformation was evaluated to be 10^3 J/mol at 773 K.

© 2017 Acta Materialia Inc. Published by Elsevier Ltd. All rights reserved.

1. Introduction

Microstructural control via phase transformations improves mechanical properties of steels drastically. In particular, the solid-solid phase transformation between face-centered cubic austenite (fcc-γ) and body-centered cubic ferrite (bcc-α) is the most important for the microstructural control of structural steels. Therefore, so far, many experimental researches for Fe-base multi-component systems have been conducted to precisely understand the phase equilibrium between the fcc-γ and bcc-α phases. Of these systems, the binary Fe-Ni system has been investigated for a long time [1–6,10], because Ni is one of the most important austenite-former elements used for high alloy steels, such as austenitic stainless steels and maraging steels. For realization of equilibrium fcc + bcc two-phase microstructure in a Fe-Ni alloy, isothermal holding at an intercritical temperature in the fcc + bcc two-phase region after solid-solution treatment is generally conducted in order to precipitate the bcc phase in the fcc matrix. However, the growth of precipitates of the bcc phase is controlled by very slow Ni diffusion in the fcc matrix, and thus the equilibrium state is not readily achieved by a heat treatment route promoting fcc-bcc forward transformation within realistic times. Therefore, in practice, the equilibrium fcc + bcc two-phase microstructure is obtained by bcc-fcc reverse transformation [7]. For the reverse transformation, a Fe-Ni alloy is quenched after solid-solution treatment and then annealed at an intercritical temperature to precipitate the fcc phase in the bcc matrix, because Ni diffusion in the bcc phase is much faster than that in the fcc phase [8]. However, it should be noted that Fe-Ni alloys have lath or lenticular martensitic microstructure after quenching, because quench hardenability of Fe is effectively enhanced by Ni addition. Thereby, previous researches for Fe-Ni phase diagram provide information on the phase boundary between the fcc-γ and bcc-martensite (bcc-α′)[2] but not that on the phase boundary between the fcc-γ and bcc-α. Considering that the martensite contains lattice defects with high density, i.e. dislocations and grain boundaries, due to lattice invariant deformation in non-thermoelastic martensitic transformation, it is unclear whether the bcc-α′ can be regarded as the bcc-α from a view-point of thermodynamics. In order to dissolve this issue, it is reasonable to obtain the two-phase microstructure consisting of fcc-γ and bcc-α. Furthermore, the martensite is easily recrystallized by cold deformation. Enomoto and Furubayashi [9] reported that cold rolling followed by annealing lead to recrystallization of lath martensite before onset of austenite reversion in Fe-Ni alloys, and eventually, fine two-phase microstructure consisting of recrystallized-ferrite and reversed-austenite was formed. In the present study, the two-phase equilibrium state of fcc-γ and bcc-α was realized by prior cold deformation of the martensite in the Fe-

* Corresponding author.
E-mail address: nakada.n.aa@m.titech.ac.jp (N. Nakada).
[1] Now at Isuzu Motors Limited.

[2] Although iron martensite has body-centered tetragonal (bct) crystal structure when interstitial carbon and nitrogen are supersaturated, interstitial-free iron-nickel martensite where solute carbon and nitrogen are precipitated as carbonitride is characterized as bcc crystal structure.

http://dx.doi.org/10.1016/j.scriptamat.2017.05.050
1359-6462/© 2017 Acta Materialia Inc. Published by Elsevier Ltd. All rights reserved.

Ni system, and then the fcc + bcc two-phase region was determined reliably. In addition, the difference in thermodynamics between the bcc-α and bcc-α′ was discussed on the basis of the experimental result.

2. Experimental procedures

Binary Fe-Ni alloys with Ni concentrations of 4, 8, 12 and 16 mass% were prepared by argon arc melting. Here, 0.1 mass% of Ti was added to each alloy to fix small amounts of C and N as carbonitride, because C and N are strong austenite-former elements affecting phase equilibrium between the fcc and bcc phases. After sufficient homogenization at 1423 K, the Fe-Ni alloys were subjected to solid-solution treatment at 1273 K for 1.8 ks, followed by water-quenching. The solution-treated alloys were cold-rolled at 95% in thickness reduction and then annealed at 773 K for various times up to 1.26 Ms. (14.6 days). The annealing temperature is lower than the start temperature of martensitic reversion, approximately 900 K in Fe-16Ni alloy [6]. The microstructure was characterized by an electron backscatter diffraction (EBSD) technique with a field emission scanning electron microscope (FE-SEM, JSM-7001F developed by JEOL). The EBSD patterns were analyzed with a dedicated software (OIM analysis ver. 7.1 developed by TSL solutions), and the volume fraction of each phase was evaluated from the EBSD phase map. Partitioning of Ni between the fcc and bcc phases was analyzed by energy dispersive X-ray spectrometry (EDX) with the FE-SEM. The FE-SEM observation for EBSD and EDX was conducted along the transverse direction of cold rolling.

3. Results and discussion

As the starting microstructure after solid-solution treatment, it was confirmed that Fe-4Ni alloy exhibited massive ferritic microstructure, and the other alloys indicated lath martensitic single microstructure owing to sufficient quench hardenability. Fig. 1 shows the inverse pole figure maps (a-d) and the phase maps (e-h) of Fe-4Ni, Fe-8Ni, Fe-12Ni and Fe-16Ni alloys, respectively, annealed at 773 K for 180 ks (2.08 days) after 95% cold rolling. In Fig.1, black lines denote high-angle grain boundaries with misorientation angle higher than 15 degrees. The inverse pole figure maps (a-d) show that all the alloys had equiaxial grained ferritic microstructure in spite of the difference in the starting microstructure. The mean ferrite grain sizes for Fe-12Ni and Fe-16Ni alloys (c, d) were smaller than those for Fe-4Ni and Fe-8Ni alloys (a, b). In response to the difference in the ferrite grain size, it is found in the phase maps that a certain amount of the austenite (green) were finely distributed in the ferrite matrix (red) in Fe-12Ni and Fe-16Ni alloys (g, h). These results reveal that the massive ferrite and the lath martensite recrystallized to the ferrite in the early stages of annealing before the onset of austenite nucleation and then the nucleated austenite grains pinned grain growth of the recrystallized-ferrite matrix. The dependencies of the volume fraction V_A of austenite on the annealing t at 773 K for cold-rolled Fe-8Ni and Fe-16Ni alloys are shown with solid and open circles, respectively, in Fig. 2. As can be seen, the fraction V_A gradually increases with increasing annealing time t, because the austenite reversion takes place via diffusional mechanism. Eventually, the volume fraction reaches to the maximum values of $V_A = 0.01$ and 0.24 for Fe-8Ni and Fe-16Ni alloys, respectively, at annealing times longer than 1 Ms. (11.6 days), meaning the achievement of thermal equilibrium state. On the other hand, horizontal dashed lines in Fig. 2 represent the corresponding values calculated with *Thermo-calc*. The calculation gives $V_A = 0.14$ and 0.51 for Fe-8Ni and Fe-16Ni alloys, respectively. Therefore, the values of V_A are much smaller for the experiment than for the calculation. Furthermore, the Ni concentrations for the bcc and fcc phases was evaluated to be 7.7 and 41 mass%, respectively, according to lever rule and the Ni partitioning behavior was confirmed by the EDX measurement of Fe-16Ni alloy for

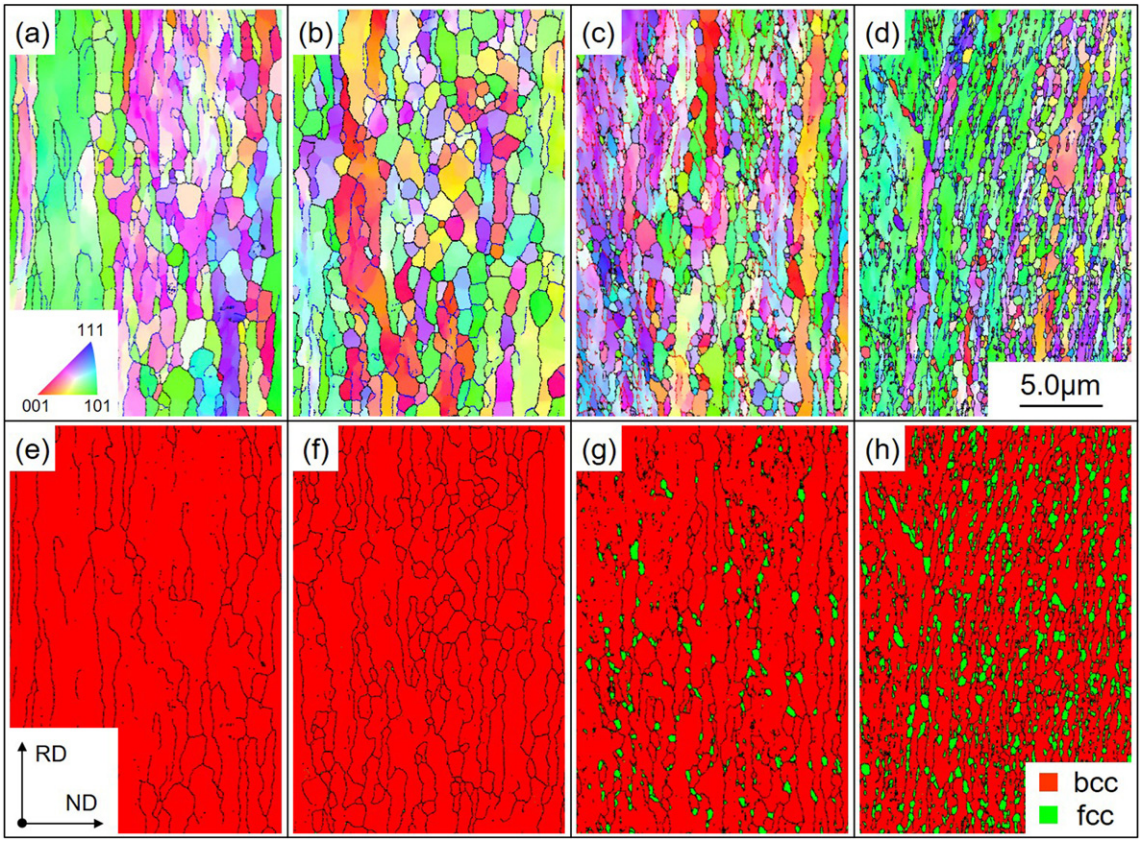


Fig. 1. Inverse pole figure and phase maps of Fe-Ni alloys annealed at 773 K for 180 ks after cold rolling with 95% in thickness reduction: (a,e) Fe-4Ni, (b,f) Fe-8Ni, (c,g) Fe-12Ni, (d,h) Fe-16Ni alloys.

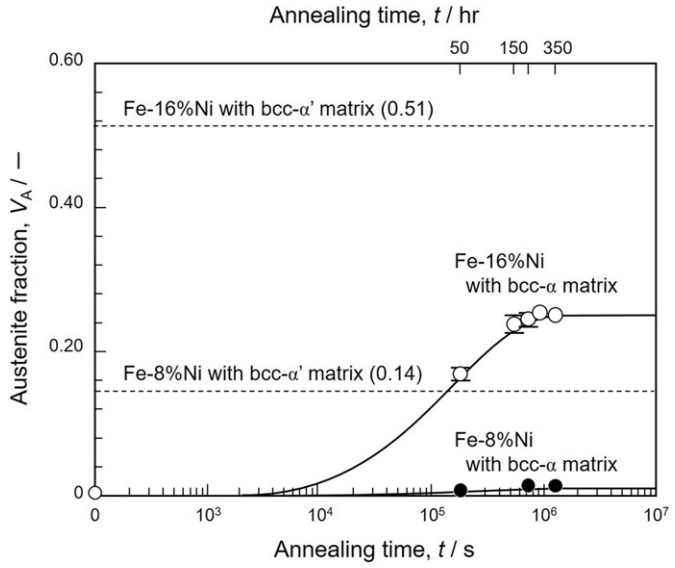


Fig. 2. Volume fraction V_A of austenite versus annealing time t at 773 K for cold-rolled Fe-8Ni and Fe-16Ni alloys.

$t = 1.26$ Ms. In contrast, according to a Fe-Ni phase diagram [4,6], the Ni concentration is 5.0 and 28 mass% for the bcc and fcc phases, respectively, at 773 K. This proves that the martensite is less stable than the ferrite, even though they have the same bcc crystal structure. Ohnuma et al. [10] also proved the similar result using powder sintered Fe-Ni alloys and emphasized that it becomes more remarkable at temperatures lower than 773 K.

The difference in phase stability between the bcc-ferrite and bcc-martensite is discussed in terms of thermodynamics with molar Gibbs energy G_m curves at 773 K in Fig. 3. Dashed curves show the results of $G_m^{fcc-\gamma}$ and $G_m^{bcc-\alpha'}$ for the fcc and bcc phases, respectively, calculated with *Thermo-calc.*, and solid curves indicate those of $G_m^{fcc-\gamma}$ and $G_m^{bcc-\alpha}$ for the fcc and bcc phases, respectively, reflecting the metallographic observation in the present study. In this figure, $G_m^{bcc-\alpha}$ is vertically shifted downward from $G_m^{bcc-\alpha'}$ in order to satisfy the Ni concentrations of 7.7 and 41 mass% for the bcc and fcc phases, respectively. As shown in Fig.1, the mean grain size of the reversed austenite is about 0.4 μm. Thus,

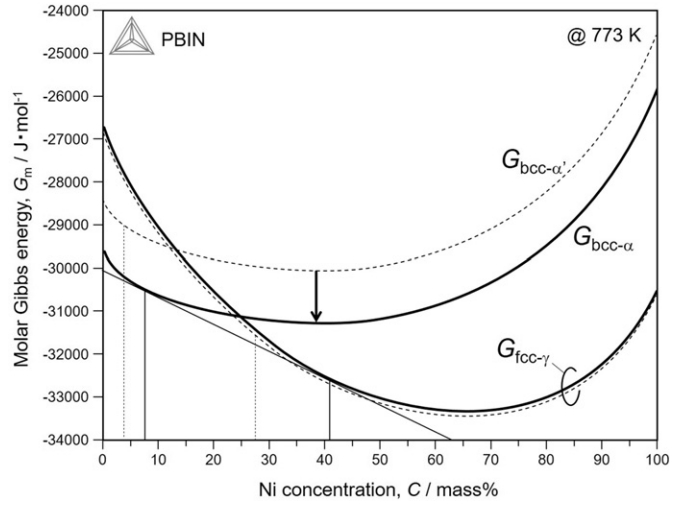


Fig. 3. Molar Gibbs energy curves in the Fe-Ni system. Dashed curves show results of fcc-γ and bcc-α′ calculated with Thermo-calc., and solid curves indicate those of fcc-γ and bcc-α satisfying the observations.

the solid curve of $G_m^{fcc-\gamma}$ is vertically moved upward by 70 J/mol to take into account of Gibbs-Thomson effect ΔG_m^{σ} described by Eq. (1).

$$\Delta G_m^{\sigma} = \frac{2\sigma V_m}{r} \tag{1}$$

Here, σ is the γ/α interfacial energy per unit area, and r and V_m are the curvature radius and molar volume, respectively, of the fcc phase. Inserting $\sigma = 1.0$ J/m^2 [11,12], $r = 2 \times 10^{-7}$ m and $V_m = 7.09 \times 10^{-6}$ m^3/mol into Eq. (1), we obtain $\Delta G_m^{\sigma} = 70.9$ J/mol. This estimation demonstrates that the value of $\Delta G_m = G_m^{bcc-\alpha'} - G_m^{bcc-\alpha}$ indicated with a bold arrow in Fig.3 is 10^3 J/mol. Iron martensite contains a lot of lattice defects, dislocations and grain boundaries, due to lattice invariant deformation on non-thermoelastic martensitic transformation. The stored energy per unit volume caused by dislocation E_{dis} and by grain boundary E_{gb} can be estimated by Eqs. (2) and (3), respectively, on the assumption of development of plate-like microstructure.

$$E_{dis} = \rho \mu b^2 V_m \tag{2}$$

$$E_{gb} = \frac{\sigma_{gb} V_m}{W} \tag{3}$$

Here, ρ, μ, b, σ_{gb} and W are dislocation density, shear modules, Burgers vector, grain boundary energy per unit area and the average width of plate-like microstructure in martensite. Given that ρ is 7.0×10^{15} m^{-2} which corresponds to a dislocation density as quenched state [13], E_{dis} is 186 J/mol at 773 K with $\mu = 60$ GPa [14] and $b = 0.25$ nm. On the other hand, lath martensite is characterized as plate-like microstructure composed of hieratical substructures, i.e. lath and block [15]. E_{gb} of low angled lath boundary is estimated to be 2.8 J/mol by substituting $\sigma_{gb} = 0.2$ J/m^2 [11] and $W = 0.5$ μm, while E_{gb} of high angled block boundary is 0.85 J/mol by $\sigma_{gb} = 1.2$ J/m^2 [11] and $W = 10$ μm. The sum of E_{dis} and E_{gb} reaches over 190 J/mol, but it is much lower than 10^3 J/mol. Considering that the dislocation density decreases rapidly during intercritical annealing due to recovery, this estimation suggests that the energy difference between ferrite and martensite is not attributed to these lattice defects.

Recently, Cong et al. [16] simulated martensitic transformation by Phase-filed simulation based on two types of slip deformation model and evaluated evolution of energy density in Fe-0.1C alloy. As a result, they reported that elastic strain energy of 1.3×10^3 J/mol is stored in lath martensite and this value is much larger than the energy derived from lattice defects, i.e. self-energy of dislocations and boundary energy. Elastic strain energy caused by internal stress is generated when eigenstrain is inhomogeneously distributed in microstructure. In martensitic transformation, several martensite variants are formed from a parent phase. Since the martensite variants have individual anisotropic transformation strain due to a lattice correspondence, martensite has an inhomogeneous microscopic distribution of eigenstrain which corresponds to the distribution of martensite variants, although the formation of several martensite variants, so-called multi-variant transformation, makes eigenstrain isotropic from a macroscopic viewpoint, as schematically illustrated in Fig. 4. This is the origin of large elastic strain energy in martensite. From this view point, recrystallized-ferrite should have little elastic strain energy because martensitic structure consisting of multi variants disappears completely through recrystallization. Of course, the internal stress and the elastic strain energy in martensite can be relaxed by atomic diffusion during annealing. Onaka et al. [17] investigated the relaxation kinetics of the internal stress by local interface diffusion and long-range volume diffusion on the basis of micromechanics. According to their investigation, the internal stress caused by volume change must be relaxed by long-range volume diffusion of atoms or vacancies, and hence the relaxation time τ can

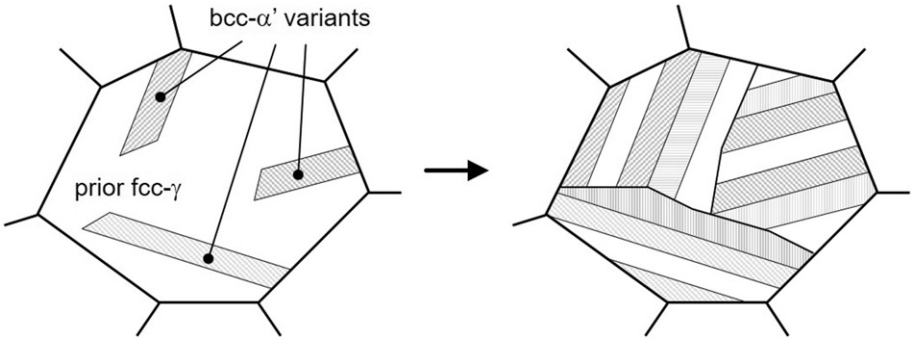


Fig. 4. Schematic illustration showing evolution of heterogeneous distribution of eigenstrain in lath martensite.

be described by the following equation.

$$\tau = \frac{a^2}{4}\frac{(1+\nu^*)\mu^* + 2(1-2\nu^*)\mu}{(1+\nu^*)\mu\mu^*}\frac{kT}{D_v\Omega} \tag{4}$$

Here, a is the diameter of second-phase inclusion with spherical shape, ν and ν^* are the Poisson's ratios of the matrix and the inclusion, respectively, μ and μ^* are the shear moduli of the matrix and the inclusion, respectively, k is Boltzmann constant, T is the temperature, D_v is the self-diffusion coefficient, and Ω is the atomic volume. Assuming $\nu^* = \nu$ and $\mu^* = \mu$, we obtain the following equation from Eq. (4)

$$\tau = \frac{a^2}{4}\frac{3(1-\nu)}{(1+\nu)\mu}\frac{kT}{D_v\Omega} \tag{5}$$

If we assume that the value of a corresponds to the width of martensite block of 10 μm, τ is estimated to be 91 Ms. (1053 days) at 873 K with $\nu = 0.3$, $\mu = 55$ GPa [12], $Dv = 1.0 \times 10^{-20}$ m^2/s [18], $\Omega = 8.2 \times 10^{-30}$ m^3 of bcc-Fe and $k = 1.38 \times 10^{-23}$ J/K. Furthermore, Onaka et al. [17] proposed that the eigenstrain ε_{ij} decreases depending on time t in accordance with the following equation.

$$\varepsilon_{ij} = \varepsilon^*_{ij}\exp\left(-t/\tau\right) \tag{6}$$

Here, ε^*_{ij} is the initial eigenstrain. Romig et al. [5] reported that an annealing time of 10.97 Ms. (127 days) is needed to realize the equilibrium state of fcc + bcc two-phase microstructure in a Fe-Ni alloy at 873 K, when reversed austenite precipitates in the martensite matrix. However, considering that elastic strain energy is roughly proportional to the square of ε^*_{ij}, Eqs. (5) and (6) reveal that 80% of the initial elastic strain energy still remains even for an annealing time of 10.97 Ms. Thus, it is nearly impossible to fully reduce elastic strain energy in lath martensite even after long time annealing. These experimental results let us know the fact that the bcc phase is sometimes strongly affected by elastic strain energy for the present phase diagrams in Fe-Ni system. In addition, this problem would affect the precipitation behavior of carbide and nitride in the martensite matrix in tempering, as well as austenite. Consequently, further investigation is needed also for other Fe-base systems.

4. Conclusions

In order to obtain reliable information on the phase equilibrium between the fcc and bcc phases in binary Fe-Ni system, cold rolling was conducted for various Fe-Ni alloys to promote recrystallization of martensite matrix. The obtained results are as follows:

(1) Lath martensite is rapidly recrystallized to ferrite by heavy cold rolling and following annealing. As a result, the fine duplex microstructure composed of recrystallized-ferrite and reversed-austenite is developed during intercritical annealing at 773 K.
(2) The equilibrium volume fraction of austenite in the recrystallized-ferrite is much smaller than that of austenite in the tempered-martensite. This suggests that the martensite is less stable than the ferrite. Their difference in molar Gibbs energy is evaluated to be 10^3 J/mol at 773 K.
(3) The increment of molar Gibbs energy in the martensite originates from the elastic strain energy, which is generated by formation of various martensite variants with individual anisotropic eigenstrain. Since long-range atomic diffusion is required to relax the elastic strain in the martensite, it is impossible in reality to completely reduce the elastic strain energy during intercritical annealing.

Acknowledgements

This study was supported by Japan Science and Technology Agency under “Collaborative Research Based on Industrial Demand, Heterogeneous Structure Control”. We would like to thank Prof. Susumu Onaka at Tokyo Institute of Technology for useful discussions and comments.

References

[1] E.A. Owen, A.H. Sully, Philos. Mag. 27 (1939) 614–636.
[2] E.A. Owen, A.H. Sully, Philos. Mag. 31 (1941) 314–338.
[3] E.A. Owen, Y.H. Liu, J. Iron Steel Inst. 163 (1949) 132–137.
[4] J.I. Goldstein, R.E. Ogilvie, Trans. Soc. AIME 223 (1965) 2083–2087.
[5] A.D. Romig Jr., J.I. Goldstein, Met. Trans. A 11 (1980) 1151–1159.
[6] L.J. Swartzendruber, V.P. Itkin, C.B. Alcock, J. Phase, Equilibria 12 (1991) 288–312.
[7] N.P. Allen, C.C. Earley, J. Iron Steel Inst. 166 (1950) 281–288.
[8] N. Nakada, K. Mizutani, T. Tsuchiyama, S. Takaki, Acta Mater. 65 (2014) 251–258.
[9] M. Enomoto, E. Furubayashi, Mater. Sci. Eng. 24 (1976) 123–129.
[10] I. Ohnuma, et al., CALPHAD XL, 2011 87.
[11] D. Wolf, Philos. Mag. 62 (1990) 447–464.
[12] M.C. Inman, H.R. Tipler, Metall. Rev. 8 (1963) 105–166.
[13] S. Takaki, K.L.N. Huynh, N. Nakada, T. Tsuchiyama, ISIJ Int. 52 (2012) 710–716.
[14] JSME, Data Book, The Modulus of Elasticity of Metals and Alloys, The Japan Society of Mechanical Engineers, Tokyo, 2001.
[15] S. Morito, X. Huang, T. Furuhara, T. Maki, N. Hansen, Acta Mater. 54 (2006) 5323–5331.
[16] Z. Cong, Y. Murata, Y. Tsukada, T. Koyama, Philos. Mag. 93 (2013) 1073–1747.
[17] S. Onaka, M. Kato, Mater. Sci. Eng. A 146 (1991) 217–232.
[18] H. Oikawa, Tetsu to Hagane 68 (1982) 1489–1497.